Available online at www.sciencedirect.com

SciVerse ScienceDirect

Energy Procedia 37 (2013) 5387 – 5402

Energy Procedia

GHGT-11

Molecular dynamics simulation of water/CO_2-quartz interfacial properties: application to subsurface gas injection

Jack McCaughan[a], Stefan Iglauer[b,*2], Fernando Bresme[c,d,*1]

[a]*Imperial College London, Department of Earth Science and Engineering, SW7 2AZ London, UK*
[b]*Curtin University, Department of Petroleum Engineering, 26 Dick Perry Avenue, 6151 Kensington, Australia*
[c]*Imperial College London, Department of Chemistry, SW7 2AZ London, UK*
[d]*Department of Chemistry, Norwegian University of Science and Technology, Norway*

Abstract

Global warming due to Carbon Dioxide (CO_2) emissions from fossil fuel consumption remains an extremely difficult problem to mitigate. One of the many purposed methods to tackle rising emissions of CO_2 is subsurface injection into geological formations known as Carbon Capture and Storage (CCS).

A major challenge, that projects involving subsurface gas injection have, is predicting the amount of gas that will be trapped in the formation effectively and safely. A major contributing factor to this uncertainty is the lack of accurate experimental data on contact angles between the subsurface rocks, formation water and CO_2. The two main difficulties with employing experimental work to estimate these parameters are the existence of partially contradicting results and the difficulty in accurately recreating the range of subsurface conditions in the laboratory. Molecular dynamics computer simulations provide a microscopic approach to recreate subsurface conditions and to explain experimental contradicting results.

We report here molecular dynamics investigations on the influence of divalent salts on the CO_2/water/quartz contact angle. We also investigate N_2/water/quartz and H_2S/water/quartz systems, in order to assess the impact that the gas has on the contact angles. The quartz surface used for these simulations was a fully coordinated quartz crystal. In addition, we present results for a hydroxylated quartz crystal model, which we have developed for this work. The dependence of the contact angles on the degree of hydroxylation is discussed.

Keywords: contact angle; structural trapping; residual trapping; wettability; molecular dynamics; carbon geo-sequestration

*1 Corresponding author. Tel.: +44-207-594-5886; *E-mail address:* f. bresme@imperial.ac.uk; *2 Tel.: +61-8-9266-7703; *E-mail address*: stefan.iglauer@curtin.edu.au

1876-6102
doi:10.1016/j.egypro.2013.06.457

1. Introduction

Increasing levels of atmospheric anthropogenic Carbon Dioxide (CO_2) since the industrial revolution have been widely considered as a principal cause of rising global temperatures [1]. Carbon Capture and Storage (CCS) has been proposed and reviewed as a possible way to mitigate these CO_2 emissions from fossil fuel consumption. The International Energy Agency predicts that CCS could account for up to a 19% reduction of global CO_2 emissions [2]. Currently in CCS projects CO_2 has been taken from gas processing schemes and injected into the subsurface for Enhanced Oil Recovery in depleting oil fields such as Shute Creek, USA [3]. Alternatively it has been injected into a nearby saline aquifer for disposal such as in the Sleipner field, Offshore Norway [4]. Hydrogen sulfide (H_2S) is another gas with negative environmental impacts commonly referred to as acid gas. It has also been injected into the subsurface for disposal by many operators [5]. This is due to the normal process of disposal, the Claus process, becoming less economical [6] in recent times.

For the injected gas to remain in the subsurface, it must be trapped sufficiently, i.e. to an extent where the effective permeability of the gas must be approximately zero. Generally, there are four main mechanisms contributing towards the trapping of CO_2 in subsurface formations:

1. Structural trapping, where a layer of rock (commonly referred to as the caprock) is present with a
   seal, which has negligible permeability. This then prevents the buoyant gas from flowing upwards [6].
2. Residual trapping, also known also as capillary trapping, where the gas is trapped as bubbles by
   capillary forces present in the pore space of the rock [8,9].
3. Dissolution trapping; where the injected CO_2 dissolves into formation brine. The brine now saturated with CO_2 sinks due to an increase in density [10,11];
4. Mineral trapping; where the CO_2 is trapped by reacting with host rock and minerals in the formation brine to form solid materials [12]. Note that this trapping mechanism (mineral) is considered to take place over a longer time frame in comparison with the other trapping mechanisms (structural, residual and dissolution).

The focus of this work is on predicting the extent of *Structural and Residual Trapping;* specifically how both these mechanisms depend on capillary forces. The magnitude of the capillary forces is determined by the capillary pressure, which is defined as the difference in pressure between the non-wetting and wetting phase (i.e the pressure difference across the curved interface) [13]. The Young-Laplace equation states the following:

$$\Delta P = P_c = \frac{2\gamma cos\theta}{r} \tag{1}$$

P_c (capillary pressure) is proportional to the interfacial tension (γ) between the two fluids and the cosine of the contact angle between the phases (θ) while inversely proportional to the effective radius of the pore (r), assuming the pore has a circular cross-section. Considering the force balance between capillary and buoyancy forces one gets:

$$h = \frac{P_{c,e}}{\Delta\rho g} \tag{2}$$

where $p_{c,e}$ is the capillary entry pressure of CO_2 into the caprock, $\Delta\rho$ is the difference in density between the two phases (water and CO_2 in the present case), g is the gravitational acceleration, and h is the height corresponding to the capillary rise, which quantifies the amount of buoyant gas trapped by structural trapping. Combining equations (1) and (2) results in:

$$h = \frac{2\gamma \cos\theta}{r\Delta\rho g} \quad (3)$$

See Naylor et al. [14] for a more detailed outline of the derivation and discussion on CO_2 column heights stored below caprocks.

If the CO_2 pressure is above this capillary entry pressure, the stored gas will break through the caprock. Though methods are being developed to monitor [15] and remediate [16] such leakages none has yet been truly tested or proven to work. Hence there is significant uncertainty related to structural trapping, which may lead to public acceptance problems of this approach. As a matter of fact, CCS projects have been stopped in Germany and the Netherlands because of such technical uncertainty and associated public or regulatory disapproval [17].

Residual trapping is generally considered secondary to structural trapping in terms of the importance for CCS projects. It is critical with respect to preventing migration of CO_2 and if no caprock is proven or exists [8]. In residual trapping the injected CO_2 displaces water in the reservoir, and a fraction of CO_2 is trapped by capillary forces. The process is analogous to the trapping of oil/natural gas during waterflooding in hydrocarbon reservoirs [18,19]. The extent of residual trapping generally increases with higher values of γ and lower values of brine-CO_2-rock contact angles θ, similar to what is observed in structural trapping. Residual trapping depends on the wettability [20,21], initial CO_2 saturation [22,23], rock porosity [18,24] and flooding history [25]. Iglauer et al. [18] have outlined the capillary trapping capacity (C_{trap}) of porous rock and how C_{trap} depends on porosity and the residual nonwetting-phase (CO_2) saturation. They also grade rocks according to their suitability for residual trapping of CO_2.

It should be clear from the discussion above that a good knowledge of contact angles is essential to predict the ability of residual and structural trapping mechanisms in CCS projects. Experimental works have nonetheless provided contradicting results. Also it is very difficult to accurately recreate the wide range of thermodynamic and physico-chemical conditions found in the subsurface. Molecular dynamics (MD) computer simulations offer an attractive method to tackle these problems. MD provides a microscopic view of the adsorption process, which is not always attainable via experiments. It is also flexible enough, in the sense that a wide range of experimental conditions, relevant to real CCS situations, can be recreated in a controlled way.

Nomenclature

MD	Molecular Dynamics
CCS	Carbon Capture and Storage
CO_2	Carbon Dioxide
H_2O	Water
NaCl	Sodium Chloride
Na	Sodium
Cl	Chlorine
$CaCl_2$	Calcium Chloride
Ca	Calcium
H_2S	Hydrogen Sulfide

N_2	Nitrogen
M	Molarity [mol/L]
θ	Contact Angle [degree]
γ	Interfacial Tension [N/m]
ε	Depth of Potential Well [J/mol]
σ	Distance at which the interparticle potential is zero [m]
U	interaction energy between atoms i and j [J]
q_i	charge on each atom site [C]

2. Investigations with the fully coordinated alpha quartz surface

2.1 Computational Methodology

For our initial investigations we employed the same force-fields used previously by Iglauer et al. [26]. The TIP4P-2005 potential model was selected for water [27] and the EPM2 model for CO_2 [28]. Both fluid models have been used in previous simulation studies showing good agreement with experimental data at elevated temperatures and high pressures [26,29,30]. The α-quartz surface was modelled by creating an orthorhombic unit cell, which was periodically replicated to generate a quartz slab. The slab was then equilibrated to create the fully coordinated surface (Si-O-Si bridged surface). All the simulations were performed with the package DL_POLY 2.19 [31,32].

The force field parameters for the quartz atoms are given in Table 1. The interatomic potential used consists of a coulombic and a Buckingham term, as given in equation (4) below:

$$U\ r_{ij} = \frac{q_i q_j e^2}{4\pi\varepsilon_0 r_{ij}} + A_{ij} e^{(-b_{ij} r)} - \frac{C_{ij}}{r_{ij}^6} \quad (4)$$

$U(r_{ij})$ is the interaction energy between atoms i and j, q is the charge on each atom site, e is the electron charge, ε_o is the vacuum permittivity and A_{ij}, b_{ij} and C_{ij} are constants taken from van Beest et al. [33].

The interaction potential between the water, gas (CO_2, H_2S or N_2) and ions (Ca^{2+} and Cl^-) was computed using coulombic potentials and dispersion interactions. Dispersion interactions were included using the Lennard- Jones (LJ) model,

$$U\ r_{ij} = 4\varepsilon \left[\left(\frac{\sigma}{r_{ij}} \right)^{12} + \left(\frac{\sigma}{r_{ij}} \right)^{6} \right], \quad (5)$$

where ε is the interaction strength between the atoms, σ is the effective diameter of the atom and r_{ij} is the distance between the two atoms i and j. The Lorentz-Berthelot combing rules (equations (6) and (7)) were used to obtain the interaction strength and effective diameter parameters between various atoms i and j [34]) with:

$$\sigma_{ij} = \frac{(\sigma_{ii} + \sigma_{jj})}{2} \quad (6)$$

$$\epsilon_{ij} = \sqrt{\epsilon_{ii} \varepsilon_{jj}} \quad (7)$$

The LJ parameters selected for the $CaCl_2$ were taken from Timko et al. [35], which correspond to the CHARMM force field. We modified slightly the diameter, σ_{ij}, to take into account the TIP4P-2005 model employed here.

To simulate H_2S, a rigid body model was created based on the work of Shyamal [36], for which the H-S-H angle is 91.5° and the H-S bond length of 1.365 Å. Shyamal [36] performed isothermal-isobaric simulations (N,P,T) showing good agreement with experimental coexistence data. We used this fact to obtain the fluid pressure from the density of the simulated system [37]. Note that this H_2S model was further validated by Lopez-Rendon et al. [38], who further showed that their simulations matched experimental results of the solubility of H_2S and CO_2 in water.

N_2 was modelled as a rigid dumbbell with bond length of 3.292 Å and LJ parameters taken from Kriebel et al. [39]. The model is in good agreement with experimental data at supercritical conditions but it is not as accurate in predicting the critical point (CP). However in the ranges of conditions considered in our simulations the model shows good accordance with the Equation of State (EOS) from Jacobsen et al. [40], and therefore represents a good starting point for our investigation.

In all the simulations presented in this work the molecules were simulated as rigid bodies, and the corresponding equations of motion were integrated using rotational integration algorithms [31]. The simulations were performed in the canonical ensemble at 300 K, using the Nose-Hoover thermostat.

Table 1. Outline of all the Force Field parameters taken from various sources, see above text for more details.

Buckingham potential parameters

Interaction	A(ij) [kJ/mol]	b(ij) [$Å^{-1}$]	C(ij) [$Å^6$.kJ/mol]
O-O	1.34E+05	2.76	1.69E+04
Si-O	1.74E+06	4.873	1.29E+04

Lennard-Jones potential parameters

Site	ε [kJ/mol]	σ [Å]	q [e^-]
O (water)	0.77502	3.1589	0
M (water)	0	0	-1.1128
H (water)	0	0	0.5564
C (CO_2)	0.23391	2.757	0.6512
O (CO_2)	0.66947	3.033	-0.3256
Si	0.5335	3.795	2.4
O (quartz)	0.6487	3.154	-1.2
Ca^{2+} ($CaCl_2$)	0.50208	2.734	2
Cl^- ($CaCl_2$)	0.666	4.91776	-1
S (H_2S)	2.0789	3.72	-0.248
H (H_2S)	0.0324	0.98	0.124
N (N_2)	0.3019	3.2973	0

The cutoff to truncate the dispersion interactions was set to 17Å. The Ewald summation method [41] was used to compute long-range coulombic interactions. The same cutoff, 17 Å, was employed for the real part contribution of the Ewald summations. Simulations were performed with periodic boundary conditions in the plane of the quartz slab, but one of the box's directions, along z-axis was not periodic. Instead a soft repulsive potential set in the x-y plane above the quartz surface was

applied to constrain the motion of the molecules / ions to one side of the simulation box. The force corresponding to this confining potential was harmonic,

$$f_{rep} = -k(z - z_0) \tag{8}$$

With k=1 kJ/mol (force constant). z_0 denotes the location of the repulsive potential, which was set to 55 Å above the quartz surface. This distance allows the water droplet's contact angle not to be affected by the repulsive wall as established in earlier work [26]. The time step for all simulation runs was set to 0.002 picoseconds (ps). The simulations typically involved $5x10^4$ equilibration steps and $0.5\text{-}1x10^6$ production steps.

To evaluate the contact angles the method reported by Bresme and Quirke [42] was applied. In this method the average droplet curvature is fitted to a geometrical construction, providing a route to extract the contact angle. See reference [26] for details.

2.2. Results for divalent salt-brine contact angles ($CaCl_2$ brine)

Previously Iglauer et al. [26] measured contact angles from molecular dynamics simulations with varying NaCl concentrations from 1M to 4M at 300K/4MPa. It was concluded that salinity has a minor effect on the contact angle. Experimentally the effect of salinity (NaCl) on the water contact angle is so far inconclusive. Chiquet et al. [43] measured a small decrease in the contact angle with increasing salinity. Espinoza and Santamarina [44] however reported a significant increase in contact angle with increasing NaCl concentration. To the authors' best knowledge no experimental work or molecular dynamics simulation have been performed to see how other salts, in this case divalent salts in the form of $CaCl_2$, affect the contact angle on a quartz surface. $CaCl_2$ is consistently found in reservoir formation water [45]. In order to investigate the impact of salt composition on the contact angles, we performed simulations considering $CaCl_2$ at 1M concentration. The configuration was generated by replacing some water molecules in a pre-equilibrated CO_2/H_2O/quartz system, in order to reach the desired concentration and preserving electroneutrality. The simulation temperature was set to 300 K and the number of CO_2 molecules was varied to achieve different pressures in the range 2-15 MPa. Our simulations indicate that divalent salts have a minor impact on the contact angles, hence following the same trends reported by us for monovalent salts.

Iglauer et al. [26] have demonstrated that the pressure conditions have a strong influence on the contact angle. The contact angle of the $CaCl_2$ follows a similar increase in the pressure range 2-15 MPa. We note that the high pressure range, 10-15 MPa, corresponds to the typically expected pressure scenario for storage depths at 1000-1500m. Overall the results from our simulations show that at typical subsurface storage pressures the divalent salts have a negligible effect (see Figure 1) on the contact angle, similar to the insignificant effect observed in NaCl solutions [26]. Hence, salt concentration should not be a main variable to consider in CCS projects directed to estimate the amount of residual trapping and the caprock integrity in terms of the capillary entry pressure.

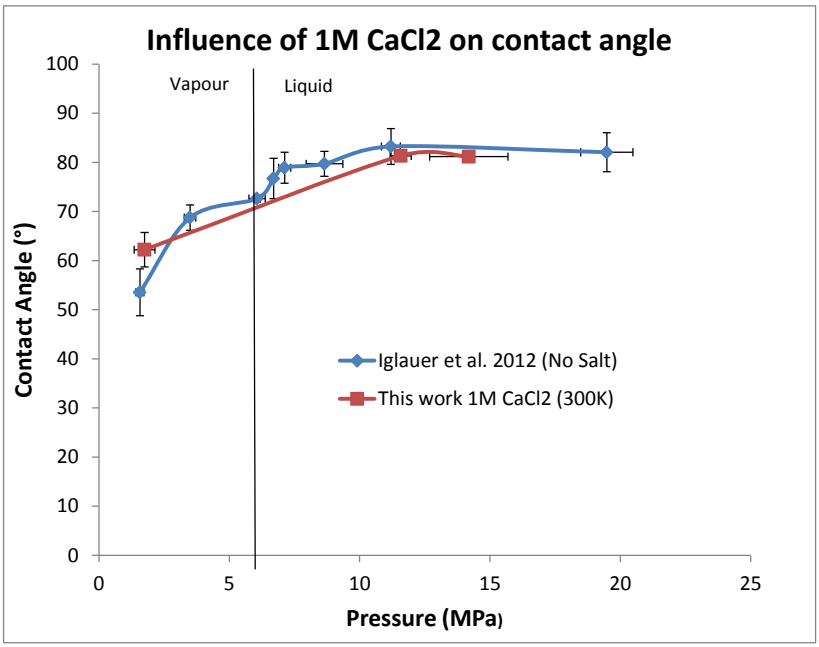

Fig. 1. Contact angle results from simulations of Iglauer et al. [26] with no salt and at 300K compared to the simulations with 1M $CaCl_2$ at 300K. The vertical line indicates the saturation pressure corresponding to the CO_2 liquid-vapour transition at 300 K.

2.3. Contact angle results for the N_2/Water/quartz system

It has been discussed recently whether Nitrogen (N_2) injection prior to CO_2 injection may aid in the evaluation of a storage site, particularly with respect to leak detection. Nitrogen gas injection is also used for enhanced oil recovery [46,47]. Hence, understanding its interfacial behaviour with quartz in the subsurface is an important issue. We therefore conducted a series of simulations to provide an initial insight into how similar water/N_2/silica contact angles compare to water/CO_2/silica contact angles. These results may be useful as a reference for future experimental work.

The highest pressure employed in the nitrogen/water/silica system was 12 MPa at 350K (Table 2). All the results up to this pressure led to a completely water wet silica surface (0º water contact angle). These results clearly indicate that N_2 has a weaker affinity for the fully coordinated quartz surface than CO_2. This is likely due to the lower van der Waals interactions of N_2 (note that the interaction strength parameter (ε) of oxygen in CO_2 is 0.66947 kJ/mol, i.e. about twice the value found for nitrogen (0.3019 kJ/mol, see Table 1). The weaker dispersive interactions in N_2 have two practical consequences; firstly, at similar pressures, N_2 possesses a much lower density than CO_2, hence fewer N_2 molecules compete with water for the surface of the fully coordinated quartz. Secondly the attraction between the fully coordinated quartz surface and N_2 is weaker as compared with CO_2. Both these effects significantly increase the surface wettability by water when N_2 is present.

Our simulations of N_2/water/silica contact angles suggest that the potential use of N_2 to test the extent of residual trapping would be a poor comparison. The test would also significantly overestimate the capillary breakthrough pressure of the caprock with respect to structural trapping. It should however be noted that N_2 may still be useful in terms of fracture detection, but this discussion is outside the scope of the present paper.

Table 2. Summary of results from simulations of N_2/H_2O/fully coordinated quartz systems. Simulations were run for a total of $5x10^4$
equilibration steps and $5x10^5$ productions steps.

Pressure [MPa]	Error [MPa]	Temperature [K]	Angle [°]	Error [°]	Comments
10	0.4	300	0	N/A	Water-wet surface
12	0.6	350	0	N/A	Water-wet surface

2.4. Contact angle results for the H_2S/Water/quartz system

Simulations for H_2S/H_2O/quartz systems were performed at 350K to compare with the corresponding CO_2/H_2O/quartz contact angles taken from our previous simulations [26]. Our results indicate that the H_2S water contact angle is larger than the analogous CO_2/H_2O/quartz contact angle at small and intermediate pressures (see Figure 2) indicating that the H_2S has a higher affinity for the quartz surface than CO_2. Our simulation corresponds to surfaces that are more hydrophobic than the ones investigated experimentally by Shah et al. [48]. The reason for these differences has been advanced in our previous work, Iglauer et al. [26]. The surface's degree of roughness is important and the surface can become chemically modified during cleaning and the actual experiment itself. In our simulations we have considered a fully coordinated α-quartz surface. However, a quartz surface in a reservoir very likely contains silanol groups. This fact motivated us to construct a hydroxylated surface and to investigate how the silanol groups affect the contact angle. This issue is discussed in detail in section 3.

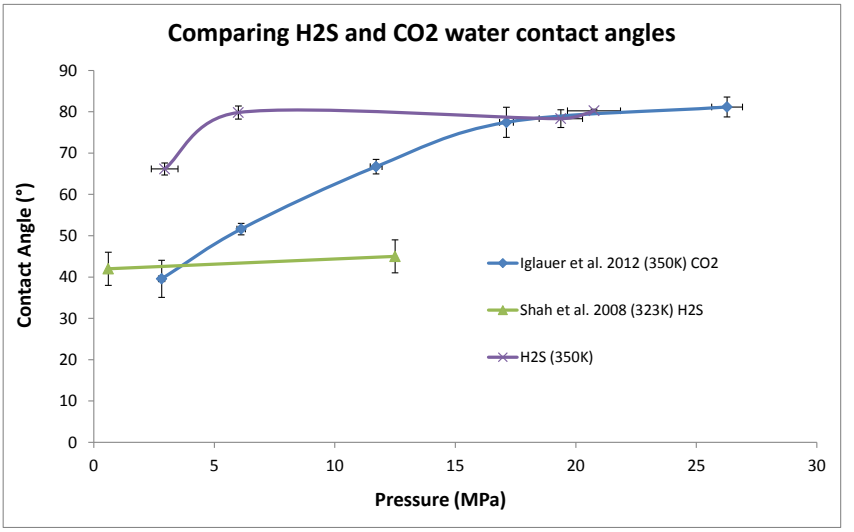

Fig. 2. H_2S/H_2O/quartz contact angle from simulations (this work) compared to experimental data from Shah et al. [48] (limited results) and simulations of the CO_2/H_2O/quartz water contact angle from Iglauer et al. [26].

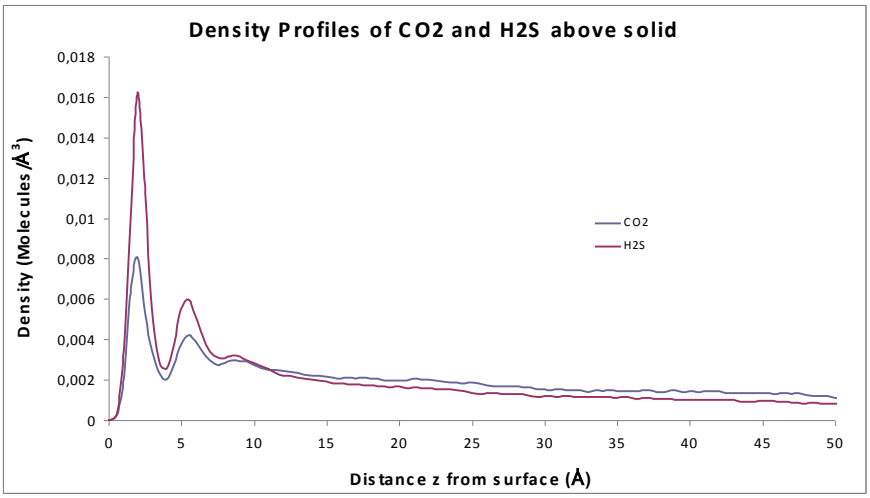

Fig. 3. Density profile of CO_2 and H_2S above the quartz surface; from the (50mol% H_2S:50mol% CO_2)/water/quartz contact angle simulation.

To gain further insight into the different adsorption behaviour of CO_2 and H_2S, we performed simulations with containing a 50mol% H_2S:50mol% CO_2 mixture/H_2O/quartz. These simulations enable a comparison of the relative wettability of H_2S and CO_2 on the quartz surface by analysing the fluid density of each molecular fluid as a function of the distance to the quartz surface (see Figure 3). Our results clearly show that H_2S has a higher affinity than CO_2 at this temperature, about twice as large. This larger affinity explains why the H_2S/H_2O/quartz water contact angles are larger than the corresponding CO_2/H_2O/quartz water contact angle. This observation of H_2S being more wetting of the crystal surface is somewhat consistent with experimental measurements on quartz and completely consistent with measurements on other surfaces, namely mica crystal and Rousee caprock. Comparing measurements from Broseta et al. [49] with Shah et al. [48] on quartz; the drainage water contact angle of CO_2/H_2O/quartz was approximately 35° at 0.1-10MPa/282K compared to drainage water contact angles of H_2S/H_2O/quartz being 42-45° at 0.6-12.5MPa/323K/0.08M NaCl brine. Shah et al. [48] observed a significant increase in drainage and imbibition water contact angles when comparing the contact angle of CO_2/H_2O to H_2S/H_2O on a mica crystal. For example the drainage water contact angle measurement on mica with CO_2 present at 1MPa/308K was 28°. Compare this to a drainage contact angle of 62° with the presence of H_2S at 1.5MPa/323K.

Overall, our results suggest that subsurface H_2S injection has less residual trapping and there will be a lower capillary break though pressure with respect to structural trapping. The simulations indicate that this difference is most apparent at low/intermediate pressures (<20MPa) and much less apparent at higher pressures (>20MPa). We note here that H_2S is a toxic and flammable gas. Exposure to concentrations exceeding 10 ppm for more than 8 hours is considered above the permissible exposure limit set by the US occupational safety and health administration [50]. It seems somewhat surprising that the general public is less concerned about H_2S with respect to subsurface injection for storage compared to CO_2 in CCS projects.

3. Development of hydroxylated alpha quartz surface

3.1 Model of the hydroylated surface and fluid adsorption

In the following we explore the impact that surface hydroxylation has on the contact angles. In this study we employed the CO_2 and H_2O models, time-step, cut-off for Van der Waals interactions, and the methodology to compute long-range coulombic interactions reported in section 2. Again, the

simulations were performed with periodic boundary conditions in the x-y plane, and a confining potential was set at a distance of 64.5 Å above the quartz surface plane (equation 8).

An orthorhombic unit cell was periodically replicated to create a quartz slab. The slab was then quenched at 1 K to create an ordered quartz crystal with a fully coordinated surface (Si-O-Si bridged surface). The top surface was hydroxylated by removing bridging oxygen atoms and then capping the newly under-coordinated silicon atoms with oxygen atoms 1.61 Å directly above them. The average Si-O bond length was 1.61 Å in the quartz crystal and so that length was selected as the Si-O bond length in the silonal groups (Si-O-H). This was also the same as the Si-O bond length used by Lee and Rossky [51]. A Si-O-H bond angle of 122.5° was used with an O-H bond length of 0.975 Å. These two parameters were taken from the work of Lopes et al. [52] who developed an empirical force field for silica with application to the quartz-water interface. This bond angle and O-H bond length has also been used elsewhere [53-55]. For the hydrogen atoms we chose a random orientation relative to the bonding oxygen by selecting a random number between φ =0-2 pi and then using the equations (9-11) to convert spherical coordinates into cartesian coordinates (θ =57.5°, r =0.975Å; see Figure 4 right):

$$x = r \sin\theta \cos\varphi \tag{9}$$

$$y = r \sin\theta \sin\varphi \tag{10}$$

$$z = r \cos\theta \tag{11}$$

The force field parameters for the quartz atoms were the same as above, namely we employed the BKS model [33]. Following the approach of Hassanali and Singer [55] the hydrogen atoms were assigned a charge of |0.6e| to ensure charge neutrality of the under coordinated surface. The LJ parameters for all the atoms were the same as before with the van der Waals interactions for the hydrogen in the silanol groups set to zero; note that these hydrogen vdW interactions are the same as those in the water model.

Zhuravlev [57] provides a good review of the extensive experimental work devoted to the hydroxylation and rehydroxylation that takes place at a silica-water interface. It states that the OH surface concentration of amorphous silica hydroxylated to the maximum degree is considered to be a physico-chemical constant of 4.6 OH/nm^2. The Zhuravlev model has stood up well to solving various applied and theoretical problems with respect to the hydroxylated silica surface. We used this fact to generate surfaces with varying degrees of hydroxylation in the range 1.7-4.5 OH/nm^2. A block of 1000 water molecules was set at 3 Å above the surface and a simulation of 5x10^3 equilibration steps and 5x10^4 production steps was performed (see Figure 4-left). Following the spreading of the water droplet on the quartz surface, we added CO_2 molecules to reach the desired pressure. We then performed a run of 5x10^4 equilibration steps and 4-5x10^5 production steps (see Figure 6, middle). Due to the surface not being large enough (98 Å by 102 Å) water molecules were first deleted from near the boundaries of the block. Water molecules were then secondly removed from the droplet itself so that 700 water molecules were left in the simulation box. The simulations were then run for a further 4-5x10^4 equilibration steps and 4-5x10^5 production steps to obtain the equilibrium contact angle of water on the quartz surface.

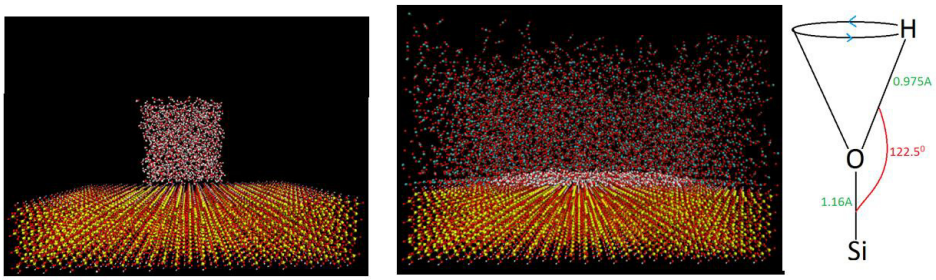

Fig. 4. (Left) Block of 1000 water molecules set approximately 3 Å above the surface. (Middle) Simulation box after $5x10^4$ equilibration steps and $0.5\text{-}1x10^6$ production steps. Once the block of water had partially wet the surface, the CO_2 were added to the simulation box. (Right) Sketch showing the Si-O-H hydroxyl group.

Various surfaces with different force field parameters were tested throughout this study. We attempted to recreate the results reported by Liu et al. [53] using a surface hydroxyl-group concentration from 1.6 OH/nm^2 (used in ref. [53]) to 4.5 OH/nm^2 (close to the maximum silanol density on an realistic silica surface [57]). Our results showed that the hydroxylated surface produces contact angles of the same order as that of our fully coordinated surface (see ref. [26]). The differences between Liu's results and ours is most likely due to the distribution of the hydroxyl groups on the silica surface, which in reference [53] leads to a quartz surface that is more hydrophobic than the one investigated by us.

Our investigations using several models for the hydroxylated quartz surface indicated that the best represenation of the surface is obtained when the hydrogen atoms on the silanol group are treated in an analogous way to hydrogens in water. A similar approach has been followed before by Cruz-Chu et al. [54]. To investigate the consistency of our model, the 1.7 OH/nm^2 hydroxylated silica surface was simulated with just CO_2 molecules present and separately simulated with 5191 water molecules placed approximately 3Å above the surface. These two simulations were repeated with the fully coordinated quartz model from Iglauer et al. [26]. All these simulations were run for a total of $2x10^3$ equilibration steps and $2x10^4$ production steps. There have been previous investigations of water and CO_2 adsorbed on quartz surfaces [51,58,59]. Lee and Rossky [51] investigated a surface with a concentration of 4.6 OH/nm^2 whereas Qin et al. [59] considered a concentration of 1.9 OH/nm^2. Our density profiles for H_2O and CO_2 (Figures 5 and 6) show similar features to those reported by these authors [51], although our models tend to predict a slightly larger adsorption. The influence of the silanol groups is evident when comparing the density profiles of the hydroxylated and fully coordinated surfaces. The latter surface results in a weaker adsorption, indicating the surface is less wettable.

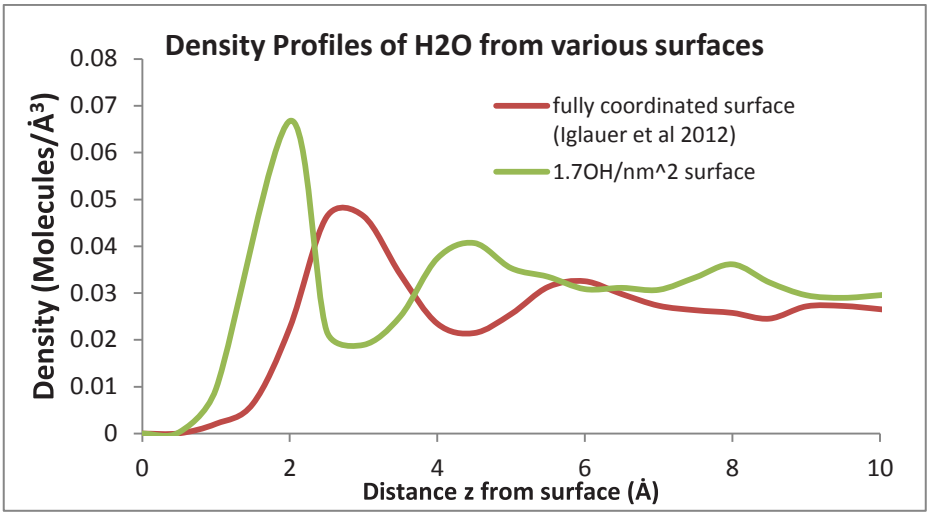

Fig 5. Water density profiles (z-direction) on the hydroxylated surface (1.7 OH/nm^2), fully coordinated silica surface from Iglauer et al. [26].

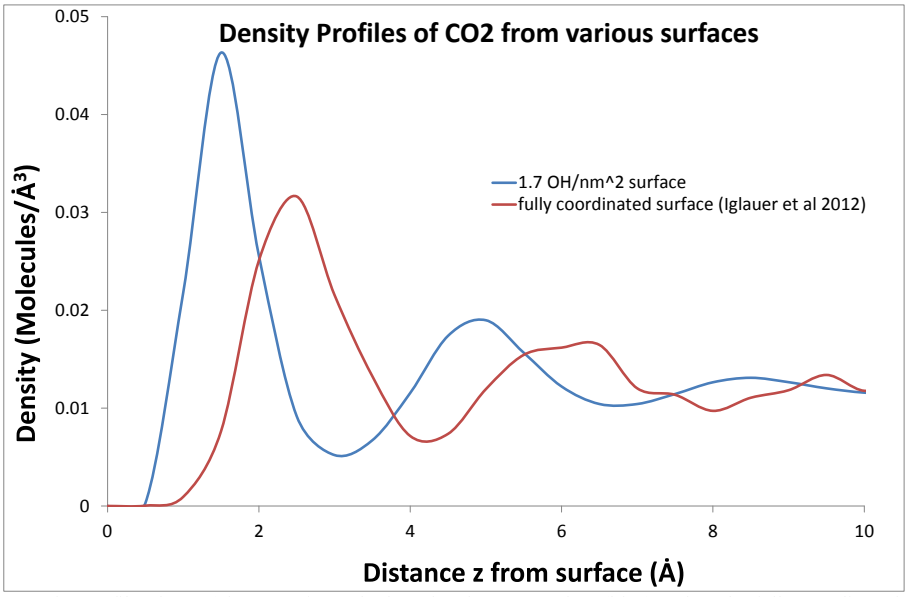

Fig. 6. Density profile of CO_2 (along z-axis) on hydroxylated quartz surface (blue) and on the fully coordinated quartz surface from Iglauer et al. [26] (red).

We have employed the model discussed above to compute the contact angle of water on the quartz surface in the presence of CO_2.We employed a quartz slab that had been previously quenched. The atomic positions in the slab were frozen throughout the simulation. CO_2 was added to reach pressures of the order of 10 MPa at 300 K. We find that the hydroxyl groups have a significant impact on the contact angle, which reduces to 55°, much lower than the angle reported by us, 80°, [26] at the same pressure and temperature for the fully coordinated surface. This increase in water wettability is consistent with an enhancement of hydrogen bonding between the water and the quartz surface, mediated by the silanol groups.

3.3. Contact angles as a function of pressure and hydroxyl group concentration on the quartz surface

The 4.5 OH/nm^2 surface was simulated at a pressure of approximately 10 MPa at 300K. The 3.7 OH/nm^2 surface was also simulated at similar conditions. Finally the lowest concentration of hydroxide on the surface was simulated (1.7 OH/nm^2) at a pressure up to 12MPa at 300K. Figures 7 and 8 show a significant decrease in the water contact angle compared to the work from Iglauer et al. [26] who performed simulations on a fully coordinated quartz surface. From Figure 7 it is clear that the contact angles on the hydroxylated quartz surface are closer to the values obtained from the range of experimental data available. Increasing the concentration of hydroxylation on the surface from 1.7-4.5 OH/nm^2 at approximately 10MPa/300K decreases the contact angle by approximately 10°. Increasing the concentration of hydroxylation on the surface from 3.7-4.5 OH/nm^2 however has a small effect on the contact angle. Our hydroxylated quartz model predicts that the CO_2/water/quartz contact angle in the subsurface is approximately 35° at 10 MPa / 300 K for high concentrations (3.7-4.5 OH/nm^2) and around 42° for lower concentrations (1.7 OH/nm^2). This means that compared to the fully coordinated surface there is a larger amount of residual trapping and a higher capillary breakthrough pressure with respect to structural trapping.

The results presented above show that changes in the OH surface concentration have a significant impact on the water/CO_2/quartz contact angles. It has to be noted that in our simulations all the silanols were fully protonated. Silanol groups can further dissociate to form Si-O$^-$. This may affect the contact angle significantly and may explain experimental measurements of a lower contact angle. The direct comparison of simulation and experimental data requires some care though. One needs to take into account that in the experiments, hysteresis is observed frequently with respect to drainage and imbibition contact angles. The hysteresis is connected to the existence of heterogeneities, chemical and structural (substrate roughness) (Broseta el al. [49]). The effect of surface roughness depends strongly on the length scale of the roughness, and can lead in the case of nanoscale roughness to either full wetting or drying. Hence, simulations provide an approach to obtain contact angles for ideal surfaces, which can be used along with phenomenological models (e.g. Cassie and Baxter equations) to take into account the impact of structural and chemical heterogeneities.

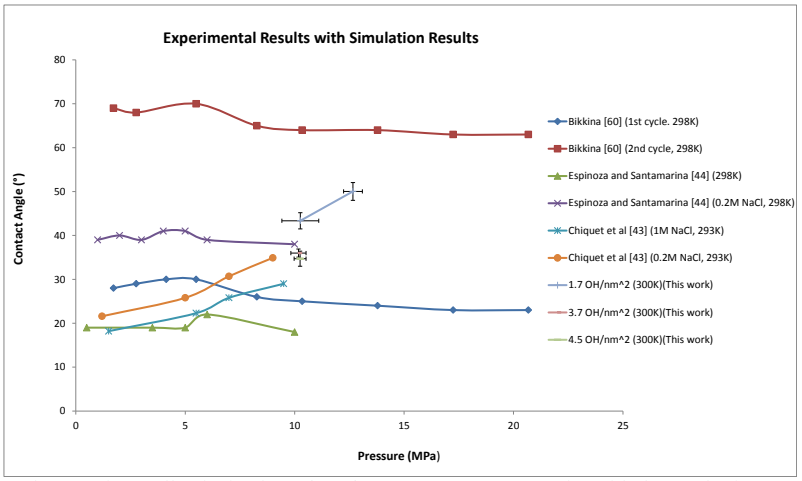

Fig. 7. Comparing the experimentally obtained CO_2/H_2O/quartz water contact angles with the results from our simulations on the hydroxylated quartz surfaces.

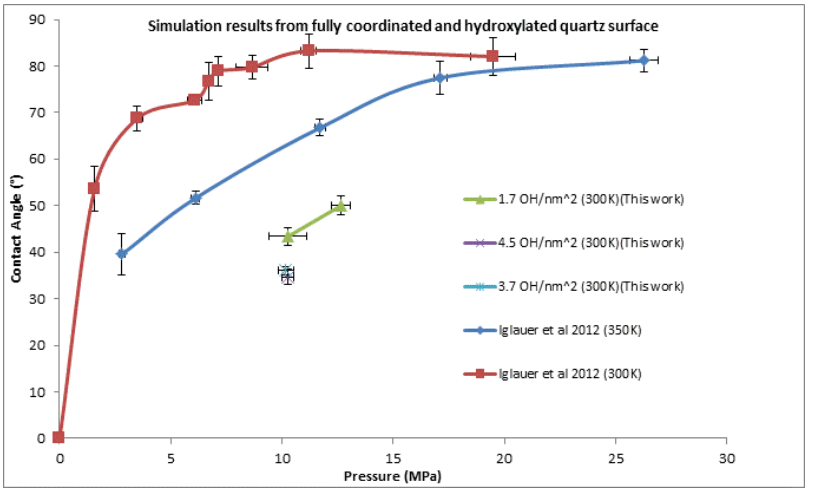

Fig. 8. Comparing simulated contact angles of CO_2/H_2O/fully coordinated-quartz [26] with the results from these simulations on the hydroxylated quartz surface.

4. Conclusions and recommendations

We present here further findings on molecular dynamics simulations performed on the fully coordinated α-quartz surface taken from Iglauer et al. [26]. We investigate the impact of divalent salts, gases (N_2, H_2S) and hydroxylation of the quartz surface on the water contact angles.

We conclude that:

- Divalent salts in the form of $CaCl_2$ have a negligible effect on the contact angle (tested at 1M concentration).
- Water spreads completely on a fully coordinated quartz surface when CO_2 is replaced by N_2.
- H_2S interacts more strongly with the quartz surface than CO_2. This leads to higher H_2S/water/quartz water contact angles as compared with CO_2/water/quartz systems under similar thermo-physical conditions.
- We have developed a consistent hydroxylated α-quartz model to measure CO_2/water/quartz contact angles that matches experimental measurements to a larger extent than the fully coordinated α-quartz surface [26]. These results highlight the relevance of surface hydroxylation in terms of determining the CO_2 storage capacity of quartz rocks.

Acknowledgements

The authors would like to thank the Imperial College High Performance Computing Service for providing computational resources.

References

[1] Mann, ME, Jones P D. Global surface temperatures over the past two millennia. *Geophys Res Lett* 2003; **30:**GL017814.
[2] International Energy Agency. Key World Energy Statistics. Paris, 2010.
[3] Shute Creek Gas Processing Facility article from Global CCS Institute (2012). Available at: http://www.globalccsinstitute.com/projects/16606; accessed August 2012
[4] Håvard A., Eiken O, Stenvold T. Monitoring gas production and CO_2 injection at the Sleipner field using time-lapse gravimetry. *Geophysics* 2008; **73:**155–161.

[5] Chakma A. Acid Gas Re-Injection- A Practical way to Eliminate CO_2 Emissions from Gas Processing Plants. *Energy Convers* 1997; **38:** S205-S209.
[6] Jamaluddin AKM., Bennion DB, Thomas FB. Acid/Sour Gas Management in the Petroleum Industry. *SPE 49522*; 1996.
[7] Hesse MA, Orr FM, Tchelepi HA. Gravity currents with residual trapping. *J Fluid Mech* 2008; **611:**35–60.
[8] Qi R, LaForce CT, Blunt MJ. Design of carbon dioxide storage in aquifers. *Int J Greenh Gas Con* 2009; **3:**195–205.
[9] Iglauer S, Paluszny A, Pentland CH, Blunt MJ. Residual CO_2 imaged with X-ray micro-tomography. *Geophys Res Lett* 2011; **38:**L21403.
[10] Riaz A, Hesse M, Tchelepi HA, Orr FM. Onset of convection in a gravitationally unstable diffusive boundary layer in porous media. *J Fluid Mech* 2006; **548:**87–111.
[11] Iglauer S. Dissolution trapping of carbon dioxide in reservoir formation brine – a carbon storage mechansim. In: Mass Transfer (ed.: Nakajima H), Rijeka: InTech 2011.
[12] Xu TF, Apps JA, Pruess K. Reactive geochemical transport simulation to study mineral trapping for CO_2 disposal in deep arenaceous formations. *J Geophys Res* 2003; **108(B2):**2071–2084.
[13] Atkins P, de Paula J. Physical Chemisty. 8th ed. *Oxford University Press*. 2009.
[14] Naylor M., Wilkinson M, Hazeldine RS. Calculation of CO_2 column heights in depleted gas fields from known pre-production gas column heights. *Mar Petrol Geol* 2011; **28**:1083.
[15] Sweatwan RE, Marsic SD, McColpin G.R. Advancements in Technology and Process Approach Reduce Cost and Increase Performance of CO_2-Flow Monitoring and Remediation. *SPE 138258*; 2010.
[16] Eke P.E, Naylor M, Haszeldine S, Curtis A. CO_2 leakage prevention technologies. *SPE 145263*; 2011.
[17] Terwel BW, ter Mors E, Daamen DDL. It's not only about safety: Beliefs and attitudes of 811 local residents regarding a CCS project in Barendrecht. *Int J Greenh Gas Con* 2012; **9:**41.
[18] Iglauer S, Wülling W, Pentland CH, Al-Mansoori SK, Blunt MJ. Capillary-Trapping Capacity of Sandstones and Sandpacks. *SPE J* 2011; **16**:778.
[19] Iglauer S, Favretto S, Spinelli G, Schena G, Blunt MJ. X-ray tomography measurements of power-law cluster size distributions for the nonwetting phase in sandstones. *Phys Rev E* 2010; **82**:056315.
[20] Spiteri EJ, Juanes R, Blunt MJ, Orr FM. A New Model of Trapping and Relative Permeability Hysteresis for all wettability characteristics. *SPE J* 2008; **13**:277.
[21] Iglauer S, Fernø M, Shearing P, Blunt MJ. Comparison of residual oil cluster size distribution, morphology and saturation in oil-wet and water-wet sandstone. *J Colloid Interf Sci* 2012; **375**: 187-192.
[22] Pentland C, El-Maghraby R, Iglauer S, Blunt MJ. Measurements of the capillary trapping of super-critical carbon dioxide in Berea sandstone. *Geophys Res Lett* 2011; **38**:L06401.
[23] Krevor S, Pini R, Zuo L, Benson SM. Relative permeability and trapping of CO_2 and water in sandstone rocks at reservoir conditions. *Adv Water Res* 2012; **48**:W02532.
[24] Tanino Y, Blunt MJ. Capillary trapping in sandstones and carbonates: dependence on pore structure. *Water Resour Res* 2012; **48**:W08525.
[25] Saeedi A, Rezaee R, Evans B, Clennell B. Mulitphase flow behaviour during CO_2 geo-sequestration: emphasis on the effect of cyclic CO_2-brine flooding. *J Petr Sci Tech* 2011; **79**:65-85.
[26] Iglauer S, Mathew MS, Bresme F. Molecular dynamics computations of brine-CO_2 interfacial tensions and brine-CO_2-quartz contact angles and their effects on structural and residual trapping mechanisms in carbon geo-sequestration", *J Colloid Interf Sci* 2012; **375**:187-192.
[27] Abascal JLF, Vega C. A general purpose model for the condensed phases of water: TIP4P/2005. *J Chem Phys* 2005; **123**:234505.
[28] Harris JG, Yung KH. Carbon Dioxide's Liquid-Vapor Coexistence Curve and Critical Properties as Predicted by a Simple Molecular Model. *J Phys Chem* 1995; **99:**12021.
[29] Nielsen LC, Bourg IC, Sposito G.. Predicting CO_2–water interfacial tension under pressure and temperature conditions of geologic CO_2 storage. *Geochim Cosmoschim Ac* 2012; **81**:28.
[30] Biscay F, Ghoufi A, Lachet V, Malfreyt P. Monte Carlo Simulations of the Pressure Dependence of the Water−Acid Gas Interfacial Tensions. *J Phys Chem B* 2009; **113**:14277.
[31] Smith W., Forester TR, Todorov IT. *DL POLY 2 USER MANUAL*. STFC Daresbury Laboratory, Daresbury, Warrington WA4 4AD, Cheshire, UK, Version 2.21, March 2010.
[32] Smith W, Forester TR. *DL-POLY 2.19*. The Council for the Central Laboratory of the Research Councils, Daresbury Laboratory at Daresbury, Nr. Warrington; 1996.
[33] van Beest BWH., Kramer G.J, van Santen RA. Force Fields for Silicas and Aluminophosphates Based on Ab Initio Calculations. *Phys Rev Lett* 1990; **64**:1955.
[34] Hansen JP, McDonald IR. *Theory of Simple Liquids*. 3rd ed. Academic, Amsterdam, 2006.
[35] Timko J, De Castro A, Kuyucak S. *Ab initio* calculation of the potential of mean force for dissociation of aqueous Ca–Cl. *J Chem Phys* 2011; **134**:204510.
[36] Shyamal K. Molecular Simulation of Vapor−Liquid Phase Equilibria of Hydrogen Sulfide and Its Mixtures with Alkanes. *J Phys Chem B* 2003; **107**:9498-9504.
[37] NIST Chemistry Webbook 2012.
[38] López-Rendón R, Alejandre J. Molecular Dynamics Simulations of the Solubility of H_2S and CO_2 in Water. *J Mex Chem Soc* 2008; **52**:88-92.
[39] Kriebel C, Müller A, Mecke M, Winkelmann J, Fischer J. Prediction of Thermodynamic Properties for Fluid Nitrogen with Molecular Dynamics Simulations. *Int J Thermophys* 1996; **17**: 1349-1363.
[40] Jacobsen RT, Stewart RB, Jahangiri M. Thermodynamic properties of nitrogen from the freezing line to 2000 K at pressures to 1000 MPa. *J Phys Chem Ref Data* 1986; **15**:735-909.

[41] Ewald P. Die Berechnung optischer und elektrostatischer Gitterpotentiale. *Ann Phys* 1921; **369**:253–287.
[42] Bresme F, Quirke N. Computer Simulation Studies of Liquid – Liquid Denses at a Liquid – Liquid Interface. *J Chem Phys* 2000; **112**:5985-5990.
[43] Chiquet P, Broseta D, Thibeau S. Wettability alteration of caprock minerals by CO_2. *Geofluids* 2007; **7**:112-122.
[44] Espinoza DN, Santamarina JC. Water-CO_2-mineral systems: Interfacial tension, contact angle and diffusion-Implications to CO_2 geological storage. *Water Resour Res* 2010; **46**:W0753.
[45] McCain WD. *Petroleum Fluids*. Tulsa: PennWell Books; 1990.
[46] Lake LW. *Enhanced oil recovery*. New Jersey: Prentice Hall; 1989.
[47] Iglauer S, Paluszny A., Blunt MJ. Simultaneous oil recovery and residual gas storage: a pore-level analysis using in-situ x-ray micro-tomography. *Fuel* 2013; **103**, 905-914in press.
[48] Shah V, Broseta D, Mouronval G.. Capillary alteration of caprocks by acid gases. *SPE 113353*, 2008.
[49] Broseta D, Tonnet N, Shah V. Are rocks still water-wet in the presence of dense CO_2 or H_2S? *Geofluids* 2012; **10**:1468-8123.
[50] U.S. Department of Health and Human Services. Toxicological Profile for Hydrogen Sulfide. pg 154, 2006.
[51] Lee SH, Rossky PJ. A comparsion of the structure and dynamics of liquid water at hydrophobic and hydrophilic surfaces-a molecular dynamics simulation study. *J Chem Phys* 1994; **100**:3334.
[52] Lopes PEM, Murashov V, Tazi M, Demchuk E, Mackerell AD. Development of an Empirical Force Field for Silica. Application to the Quartz- water Interface. *J Phys Chem B* 2006;**110**:2782-2792.
[53] Liu SY, Yang XN, Qin Y. Molecular Dynamics Simulation of wetting behaviour at CO_2/water/solid interfaces. *Chin Sci Bul* 2010; **55**:2252-2257.
[54] Cruz-Chu ER, Aksimentiev A, Schulten K. Water-Silica Force Field for Simulating Nanodevices. *J Phys Chem B* 2006; **110**:21497.
[55] van Duin ACT, Strachan A, Stewman S, Zhang Q, Xu X, Goddard WA. $ReaxFF_{SiO}$ Recative Force Field for Silicon and Silicon Oxide Systems. *J Phys Chem A* 2003; **107:**3803.
[56] Hassanali AA, Singer JS. Static and dynamics properties of the water/amorphous silica interface: a model for the undissociated surface. *J Computer-Aided Mater Des* 2006; **14**:53.
[57] Zhuravlev LT. The surface chemistry of amorphous silica. Zhuravlev model. *Colloids and Surfaces A: Physicochemical and Engineering Aspects* 2000; **173**:1-38.
[58] Notman B, Walsh RT. Molecular Dynamics Studies of the Interactions of Water and Amino Acid Analogues with Quartz Surface. *Langmuir* 2009; **25**:1638.
[59] Qin Y, Yang X, Zhu Y, Ping J. Molecular Dynamics Simulation of Interaction between Supercritical CO_2 Fluid and Modified Silica Surfaces. *J Phys Chem C* 2008; **112**:12815.
[60] Bikkina PK. Contact angle measurements of CO_2–water–quartz/calcite systems in the perspective of carbon sequestration. *Int J Greenh Gas Con* 2011; **5**:1259.